

The Pristine survey: XXVIII. The extremely metal-poor stream C-19 stretches over more than 100 degrees

Zhen Yuan (袁珍)^{1,2,3}, Tadafumi Matsuno⁴, Tatyana Sitnova⁵, Nicolas F. Martin^{3,6}, Rodrigo A. Ibata³, Anke Ardern-Arentsen⁷, Raymond Carlberg⁸, Jonay I. González Hernández^{9,10}, Erika Holmbeck¹¹, Georges Kordopatis¹², Fangzhou Jiang^{13,11}, Khyati Malhan¹⁴, Julio Navarro¹⁵, Federico Sestito¹⁶, Kim A. Venn¹⁵, Akshara Viswanathan^{15,17}, Sara Vitali¹⁸

¹ School of Astronomy and Space Science, Nanjing University, Nanjing, Jiangsu 210093, China, zhen.yuan@nju.edu.cn

² Key Laboratory of Modern Astronomy and Astrophysics, Nanjing University, Ministry of Education, Nanjing 210093, China

³ Université de Strasbourg, CNRS, Observatoire astronomique de Strasbourg, UMR 7550, F-67000 Strasbourg, France

⁴ Astronomisches Rechen-Institut, Zentrum für Astronomie der Universität Heidelberg, Mönchhofstraße 12-14, 69120 Heidelberg, Germany

⁵ Institute of Astronomy, Russian Academy of Sciences, Pyatnitskaya 48, 119017, Moscow, Russia

⁶ Max-Planck-Institut für Astronomie, Königstuhl 17, D-69117 Heidelberg, Germany

⁷ Institute of Astronomy, University of Cambridge, Madingley Road, Cambridge CB3 0HA, UK

⁸ Department of Astronomy & Astrophysics, University of Toronto, Toronto, ON M5S 3H4, Canada

⁹ Instituto de Astrofísica de Canarias, E-38205 La Laguna, Tenerife, Spain

¹⁰ Universidad de La Laguna, Departamento de Astrofísica, 38206 La Laguna, Tenerife, Spain

¹¹ The Observatories of the Carnegie Institution for Science, 813 Santa Barbara Street, Pasadena, CA 91101, USA

¹² Université Côte d'Azur, Observatoire de la Côte d'Azur, CNRS, Laboratoire Lagrange, Nice, France

¹³ Kavli Institute for Astronomy and Astrophysics, Peking University, Beijing 100871, China

¹⁴ DARK, Niels Bohr Institute, University of Copenhagen, Jagtvej 128, 2200 Copenhagen, Denmark

¹⁵ Dept. of Physics and Astronomy, University of Victoria, P.O. Box 3055, STN CSC, Victoria BC V8W 3P6, Canada

¹⁶ Centre for Astrophysics Research, Department of Physics, Astronomy and Mathematics, University of Hertfordshire, Hatfield, AL10 9AB, UK

¹⁷ Kapteyn Astronomical Institute, University of Groningen, Landleven 12, 9747 AD Groningen, The Netherlands

¹⁸ Núcleo de Astronomía, Facultad de Ingeniería y Ciencias Universidad Diego Portales, Ejército 441, Santiago, Chile

Received XXX; accepted XXX

ABSTRACT

The discovery of the most metal-poor stream, C-19, provides us with a fossil record of a stellar structure born very soon after the Big Bang. In this work, we search for new C-19 members over the whole sky by combining two complementary stream-searching algorithms, STREAMFINDER and StarGO, and utilizing low-metallicity star samples from the Pristine survey as well as Gaia BP/RP spectro-photometric catalogues. We confirm twelve new members, spread over more than 100°, using velocity and metallicity information from a set of spectroscopic follow-up programs that targeted a quasi-complete sample of our bright candidates ($G \leq 16.0$). From the updated set of stream members, we confirm that the stream is wide, with a stream width of ~ 200 pc, and dynamically hot, with a derived velocity dispersion of $11.1_{-1.6}^{+1.9}$ km s⁻¹. The tension remains between these quantities and a purely baryonic scenario in which the relatively low-mass stream (even updated to a few $10^4 M_{\odot}$) stems from a globular cluster progenitor, as suggested by its chemical abundances. Some heating mechanism, such as preheating of the cluster in its own dark matter halo or through interactions with halo sub-structures appears necessary to explain the tension. The impact of binaries on the measured dispersion also remains unknown. Detailed elemental abundances of more stream members as well as multi-epoch radial velocities from spectroscopic observations are therefore crucial to fully understand the nature and past history of the most metal-poor stream of the Milky Way.

Key words. The Galaxy – Galaxy: abundances – Galaxy: kinematics and dynamics – stars: abundances

1. Introduction

Old stellar streams are fossil relics from the very early Universe. We can find them orbiting in the nearby halo, which allows us to measure motions and chemical abundances of each individual member with great precision. Detailed chemodynamical studies of streams open the window to understanding the formation of the first stellar structures as an alternative approach to direct observations, such as the images and spectra of high redshift galax-

ies (e.g., GZH2, Zavala et al. 2024) using the James Webb Space Telescope (JWST).

As age is a quantity that is very difficult to directly measure for most stars, the iron abundance of a star, which records the chemical enrichment (or lack thereof) of their birth place, is generally used as a crude proxy for age. Extremely metal-poor (EMP) stars have $[\text{Fe}/\text{H}] < -3.0$, which is less than 1/1000th of the solar abundance. These stars are born in a pristine environment at a time supernova events occurred sparsely and the interstellar medium was not well mixed (e.g., Argast et al. 2000),

roughly ~ 1 Gyr after the big bang ($z \sim 5 - 6$). It is not hard to imagine that streams consisting of EMP stars come from stellar structures formed at the same epoch.

In the Gaia era, stellar stream searches (e.g., [Ibata et al. 2021](#)) have now revealed a handful of low-metallicity streams ([Wan et al. 2020](#); [Martin et al. 2022a](#)), the most metal-poor of which is the C-19 stream ([Martin et al. 2022b](#)). Originally identified as an EMP stream from the Pristine photometric metallicity survey, follow-up spectroscopic observations of its brightest stars confirmed the stream stars have $[\text{Fe}/\text{H}] = -3.28$, with an unresolved metallicity dispersion of less than 0.18 dex at the 95% confidence level. The latter strongly suggests that the C-19 progenitor was a globular cluster. This is also supported by the relatively large variation in light element between two members, a distinctive signature of globular clusters (see e.g., [Gratton et al. 2004](#); [Bastian & Lardo 2018](#), and references within). Previous observations have also highlighted a tension between the dynamical properties and its presumed globular cluster progenitor. C-19 has an large velocity dispersion for a cluster ($\sigma_v = 6.2^{+2.0}_{-1.4} \text{ km s}^{-1}$), with an estimated mass of only a few times $10^4 M_\odot$, based on precise velocity measurement of 10 members brighter than $G = 17.6$ ([Yuan et al. 2022b](#)). This is further consolidated by the measurements of 12 faint subgiant members ($G \approx 20$) by X-Shooter on ESO 8.2 m VLT ([Bonifacio et al. 2024](#)). C-19 is the most metal-poor system we have been able to obtain precise chemodynamical measurements for, and current data shows that it is a much more complicated structure than expected.

Previous studies also revealed a new member star separated by 30° from the main body ([Yuan et al. 2022b](#)), which opens the promise that there could be more as-of-yet undiscovered C-19 members along the orbit. From the perspective of the formation of the first stellar structures, finding more bright stars in the stream would allow us to obtain their detailed elemental abundances and characterize the nature of the stream progenitor. In this work, we report a thorough search of bright C-19 members ($G \lesssim 16.0$) over the whole sky. This task is now possible thanks to the newly released Gaia DR3 data and the XP spectra that have been used to derive metallicities over the full sky, combined with the improved search capabilities from the fusion of STREAMFINDER and StarGO ([Yuan et al. 2018](#); [Ibata et al. 2021](#); [Yuan et al. 2022a](#)). Using high-resolution spectra from telescopes in both hemispheres, we are able to confirm their memberships based on both velocity and metallicity.

The identification of candidate members is explained in detail in Sec. 2. The analysis of the metallicities of the observed candidates from combined telescope programs is described in Sec. 3. The updated dynamical properties of C-19, including all the newly confirmed members, are derived in Sec. 4. The study of the chemical signature of a sub-sample of the stars reported here will be presented in a forthcoming paper (Venn et al., in preparation).

2. Member identification

2.1. Before Gaia DR3

We first search for stars similar to known C-19 stars in dynamical space. This is done by applying StarGO to a STREAMFINDER catalog of stars likely to be in a stream, between 10 to 30 kpc. Contrary to the main Gaia EDR3 STREAMFINDER catalog ([Ibata et al. 2021](#)), we consider stars with lower probabilities, using an $8\text{-}\sigma$ instead of the $10\text{-}\sigma$ originally used by [Ibata et al. \(2021\)](#). StarGO uses a self-organizing map (SOM) to visualize the clus-

tering of these stars in the (E, L_z, θ, ϕ) space, where the latter two quantities characterize directions of the angular momentum vector:

$$\theta = \arccos(L_z/L), \quad \phi = \arctan(L_x/L_y). \quad (1)$$

The 2D neuron map trained by the STREAMFINDER catalog is shown in Fig. 1(a), where a neuron is located at each grid point (x, y) . Stars that have similar properties in dynamical space will be located close to each other on the SOM. We can then easily select stars close to the known C-19 stars on the trained SOM. Instead of re-mapping these stars using their real measurements (e.g., their radial velocities from the follow-up observations), we simply find them in the STREAMFINDER catalog shown as red crosses in Fig. 1(a), so they are more directly comparable to the other stars. This way, we are not biased by offsets that may arise between the actual velocities and the predicted ones from STREAMFINDER. This procedure is similar to the one we successfully applied to the search of Cetus stream members ([Yuan et al. 2022a](#)).

To identify new candidate C-19 stars, we first calculate the distance Δ_{C19} of each STREAMFINDER star to the ten C-19 members on the 2D map. That is $\Delta_{C19} = \sqrt{(x_{\text{SOM}} - x_{\text{SOM,C19}})^2 + (y_{\text{SOM}} - y_{\text{SOM,C19}})^2}$, whose distribution is shown in panel (b) of Fig. 1. We then select the 1% of stars that have the smallest Δ_{C19} . These stars are color coded by their proper motion in the δ direction in panels (a) and (c) of Fig. 1. Their on-sky projection (bottom panel of the Figure) immediately shows two potential stream segments (located at $\delta \sim -10^\circ$ and $\delta \sim -45^\circ$) that have the same proper motion as that of the stream orbit from [Ibata et al. \(2023\)](#). In total, there are nine stars in these segments brighter than $G = 17.5$, which we highlight with open yellow circles. After further excluding these candidates with photometric metallicities above $[\text{Fe}/\text{H}] = -2.0$ in the SkyMapper DR2 ([Huang et al. 2022](#)), Pristine catalog ([Starkenburg et al. 2017](#)), we are left with four candidates along the C-19 orbit and away from the main body for spectroscopic follow-up. These are highlighted with open black circles in panel (c) of Fig. 1. Note that two of these stars are so close together, around $\alpha = 347^\circ$, that they are almost indistinguishable in the Figure. We also tested tuning the threshold on Δ_{C19} to be more inclusive, but this does not lead to any more convincing candidates.

We observed these four most likely candidates using the Magellan telescope on 19 August 2022 (PI: Jiang), with an exposure time of 20 - 30 minutes for each of the three targets fainter than $G = 16$, and 10 minutes for the most southern one (6559328209695612544) with $G = 13.7$. We used the standard setup of the Magellan Inamori Kyocera Echelle (MIKE) spectrograph ($0.7'' \times 5.0''$ slit, 2×2 bin, standard grating angle), which reaches a resolving power $R \sim 28\,000$ and $\sim 35\,000$ in the red and blue wavelength regions, respectively ([Bernstein et al. 2003](#)). The data is reduced with the MIKE Carnegie Python pipeline ([Kelson 2003](#)). We derive their radial velocities using iSpec ([Blanco-Cuaresma et al. 2014](#); [Blanco-Cuaresma 2019](#)), by comparison with standard star HD 182572 observed during the same night. All of the candidates have velocities consistent with the C-19 orbit, shown as orange circles in Fig. 2. Two stars are located close to the member separated by 30° away from the main body, that was previously confirmed by [Yuan et al. \(2022b\)](#), and the other two are located 30° further south. Their spectra also show that they all have metallicities ≈ -3.2 , which further confirms their membership (see details in Sec. 3).

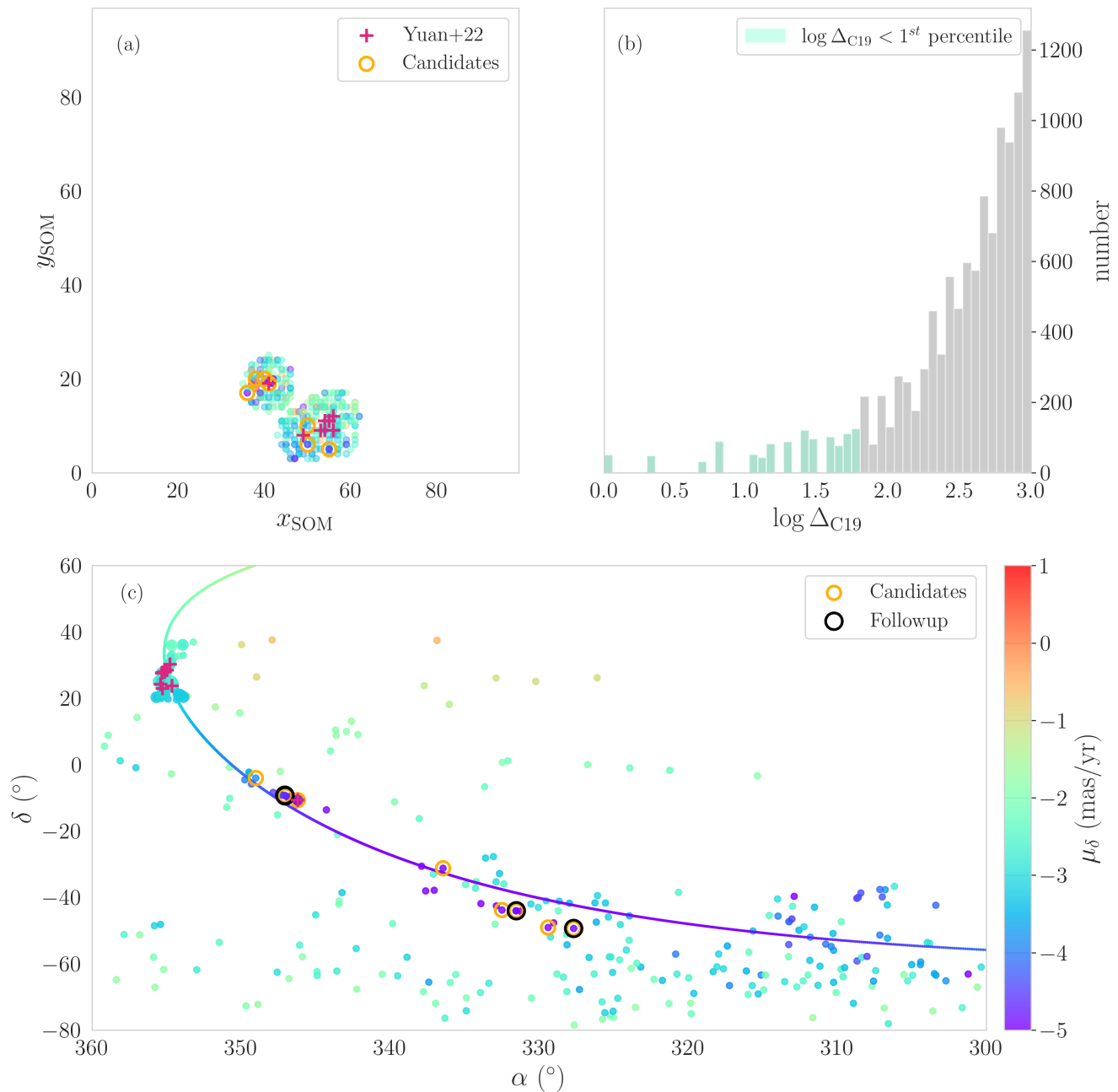


Fig. 1. (a) Self-organizing-map trained by the STREAMFINDER catalog in the space of (E, L_z, θ, ϕ) . The gray color-bar represents the differences in the weight vectors between neighboring neurons. Previously confirmed C-19 members are projected onto the SOM and plotted as red crosses. (b) Histogram of the logarithmic distances in the weight vector space between the existing C-19 stars and stars from the STREAMFINDER catalog (Δ_{SOM}). Stars below the 1st percentile are selected as candidate C-19 members and show in green in the histogram. They are also plotted as small colored circles in the other panels, with the color representing their proper motions in Gaia DR3 along the Declination direction, μ_δ . Candidates brighter than $G = 17.5$ are further highlighted by yellow circles. (c) On-sky projection of the candidate members color-coded by μ_δ . Two stream segments are identifiable with similar μ_δ . The final four candidates, selected through other means (see text) are highlighted with black circles.

2.2. After Gaia DR3

Gaia DR3 greatly expands the Radial Velocity Sample (RVS) to $G = 16$ with an average magnitude of $G \approx 14.5$ (Katz et al. 2023). Moreover, using the Ca H & K band constructed from the Gaia BP/RP spectra (Carrasco et al. 2021; Andrae et al. 2023; Montegriffo et al. 2023), we are able to estimate photometric metallicities for very metal-poor stars with $G \lesssim 16.0$ (the

Pristine-Gaia synthetic catalog Martin et al. 2024). All this new information makes it possible to do a star-by-star search for C-19 members with the knowledge of the orbit and the metallicity of the stream.

We start with stars that have Gaia RVS radial velocities, along with Pristine-Gaia synthetic metallicities $[\text{Fe}/\text{H}] < -2.8$ (using their giant photometric metallicity model). Then we select

those stars along the C-19 trajectory in the 6-D kinematic space that have differences in both tangential and radial velocities less than 30 km s^{-1} with respect to the values predicted for the orbit. This approach gives us six potential members with $G < 14.5$. Most of them are located along the two stream segments previously found, one of which is an EMP star discovered in SEGUE (Aoki et al. 2013). There is one star that is located at $\delta \approx +75^\circ$, on the other side of the Milky Way disk.

We followed up two candidates with Magellan/MIKE on August 2022 (PI: Jiang; the program already mentioned above), and one star with the Isaac Newton Telescope (INT) on 19 July 2022 (PI: Viswanathan). In the INT program, the Intermediate Dispersion Spectrograph (IDS) is equipped with the RED+2 CCD. We used the R1200R grating, a $1.37''$ slit width, and the GG495 order-sorting filter. This setting gives a resolving power of $R \sim 8000$ around the CaT region from 7850 to 9150 Å (Viswanathan et al. 2024). The one star above the disk is observed with the Subaru telescope on 20 September 2022 (PI: Yuan). In this program, we used the High Dispersion Spectrograph (HDS) in the setup of StdYd with a slit width of $0.8''$. This provides a wavelength coverage of 4000 – 5340 and 5450 – 6800 Å, $R = 45\,000$ (Noguchi et al. 2002). The data is reduced using the IRAF¹ script hdsq1². For each target, we took a quick exposure of 10 minutes, irrespective of the telescope. This allows us to derive their metallicities for further confirmation of their membership, which is described in detail in Sec. 3.

Up to now, we are confident that, in addition to the main body of the C-19 stream, there are two additional segments of the stream at lower declination, as revealed in panel (c) of Fig. 1. The previously mentioned star-by-star search approach is based on the Gaia RVS sample, which typically contains bright stars with $G < 14.5$. We believe that there should be additional fainter members that are awaiting discovery. Based on the detailed kinematics of the confirmed members in these two stream segments, we are able to do a similar star-by-star search in fainter stars that do not have radial velocity information. To do so, we use both Pristine-Gaia synthetic metallicities from Gaia BP/RP and proprietary Pristine metallicities for fainter stars. As before, we select stars with $[\text{Fe}/\text{H}] < -2.8$ and proper motions compatible with the orbit around the known segments. We found seven candidates with $14.8 < G < 17.4$ and only one of those (2641204161744171392) has a radial velocity from Gaia RVS. The velocity does agree well with expectations from the C-19 orbit at this location.

We observed these seven stars with exposure time of 10 minutes each on the nights of 2 & 4 September 2023 (PI: Ibata) using the very large telescope (VLT) with the UV-visual echelle (UVES) spectrograph. The slit width was set to be $0.7''$, which provides a resolving power $R \sim 60\,000$. The wavelength coverage is 3750 – 5000, 5700 – 7500, and 7660 – 9450 Å (Dekker et al. 2000). The observed spectra are reduced with the ESO pipeline³. We confirm that all of them have radial velocities consistent with that of the C-19 orbit at their respective positions.

With all these newly confirmed members, whose properties are shown in Fig. 2, the C-19 stream is continuously populated from the main body to $\delta = -10^\circ$. The other segment starts from $\delta = -38^\circ$ and no members are found in between. Over-

all, the stream profile is more complete above $\delta = -10^\circ$ due to the boundaries of the Pristine survey footprint. Within the Pristine footprint, the proprietary Pristine data has more accurate Ca H&K photometry and reaches fainter stars compared to the Pristine-Gaia synthetic Ca H&K from Gaia BP/RP. We therefore naturally find more fainter new members ($G \gtrsim 16$) within its sky coverage. The lack of deeper Ca H&K data in the South possibly explains the gap in the current distribution of C-19. The furthest member in the North is separated from the main body of the stream by the MW disk. It is also located in a region without overlap with the Pristine footprint.

3. Metallicity

For all the 15 stars observed in this work, we estimate the stellar parameters, the distance, and the extinction by fitting the metal-poor ($Z = 2 \times 10^{-5}$, corresponding to $[\text{Fe}/\text{H}] = -3.2$), α -enhanced BASTI-IAC isochrones (Hidalgo et al. 2018; Pietrinferni et al. 2021) to the Gaia and 2MASS photometry (Cutri et al. 2003; Skrutskie et al. 2006) as well as the Gaia parallax of the star. We maximize the likelihood by varying the distance, initial mass, age, and extinction. We use a flat prior between 10 Gyr and 14 Gyr for the age and the initial mass function by Chabrier (2003) for the mass. We added 0.05 mag error floors in quadrature to the reported uncertainties in photometry to account for possible systematic offsets between the observations and the isochrone models. The inferred stellar parameters are shown in Table 2.

Combining all the follow-up programs, there are eleven stars that have high-resolution spectra with a resolving power $R \gtrsim 30\,000$ using Subaru/HDS, Magellan/MIKE, and VLT/UVES. Among them, eight stars have sufficiently high signal-to-noise ratio (S/N) spectra for the analysis of individual Fe lines (see in Tab. 1). The five stars with UVES spectra do not have a high enough S/N for such analysis, but we are still able to infer metallicities from the Ca II triplet (CaT) lines for all of them. In order to check consistency between these two methods, we derive metallicities using the CaT lines for the nine stars with high- S/N HR spectra. The two analysis methods are briefly described below.

The first method is based on equivalent widths of individual Fe lines and stellar parameters. We first measure the equivalent widths by fitting a Gaussian profile to each Fe line. We then construct a model atmosphere by interpolating the grid of MARCS model atmospheres (Gustafsson et al. 2008), using the stellar parameters of the studied star. Since S/N is not sufficient to determine the microturbulent velocity (v_t) for most of our targets, an empirical approach is adopted here. We first fit a linear function to the relation between v_t and $\log g$ among the extremely metal-poor giants ($[\text{Fe}/\text{H}] < -2.8$, $T_{\text{eff}} < 5500 \text{ K}$, and $\log g < 3.0$) of Li et al. (2022a). The v_t values we adopt for the C-19 stars are determined from this linear relation with the estimated $\log g$. Based on these inputs (v_t , T_{eff} , $\log g$, and the equivalent widths), we derive the Fe abundance, using the radiative transfer code MOOG (Snedden 1973), from 7–57 neutral Fe lines. The uncertainties on the derived metallicities are dominated by the uncertainties on T_{eff} and are estimated to be ~ 0.1 dex.

In the second approach, we first measure the equivalent widths of the CaT lines by fitting a voigt profile to each component. We then derive the metallicity using the relation between metallicity, total equivalent width, and absolute K_s band magnitude, as calibrated by Carrera et al. (2013). The metallicity uncertainties are dominated by the scatter around the calibrated re-

¹ IRAF is distributed by the National Optical Astronomy Observatory, which is operated by the Association of Universities for Research in Astronomy (AURA) under a cooperative agreement with the National Science Foundation

² <http://www.subarutelescope.org/Observing/Instruments/HDS/hdsq1-e.html>

³ <https://www.eso.org/sci/software/pipelines/>

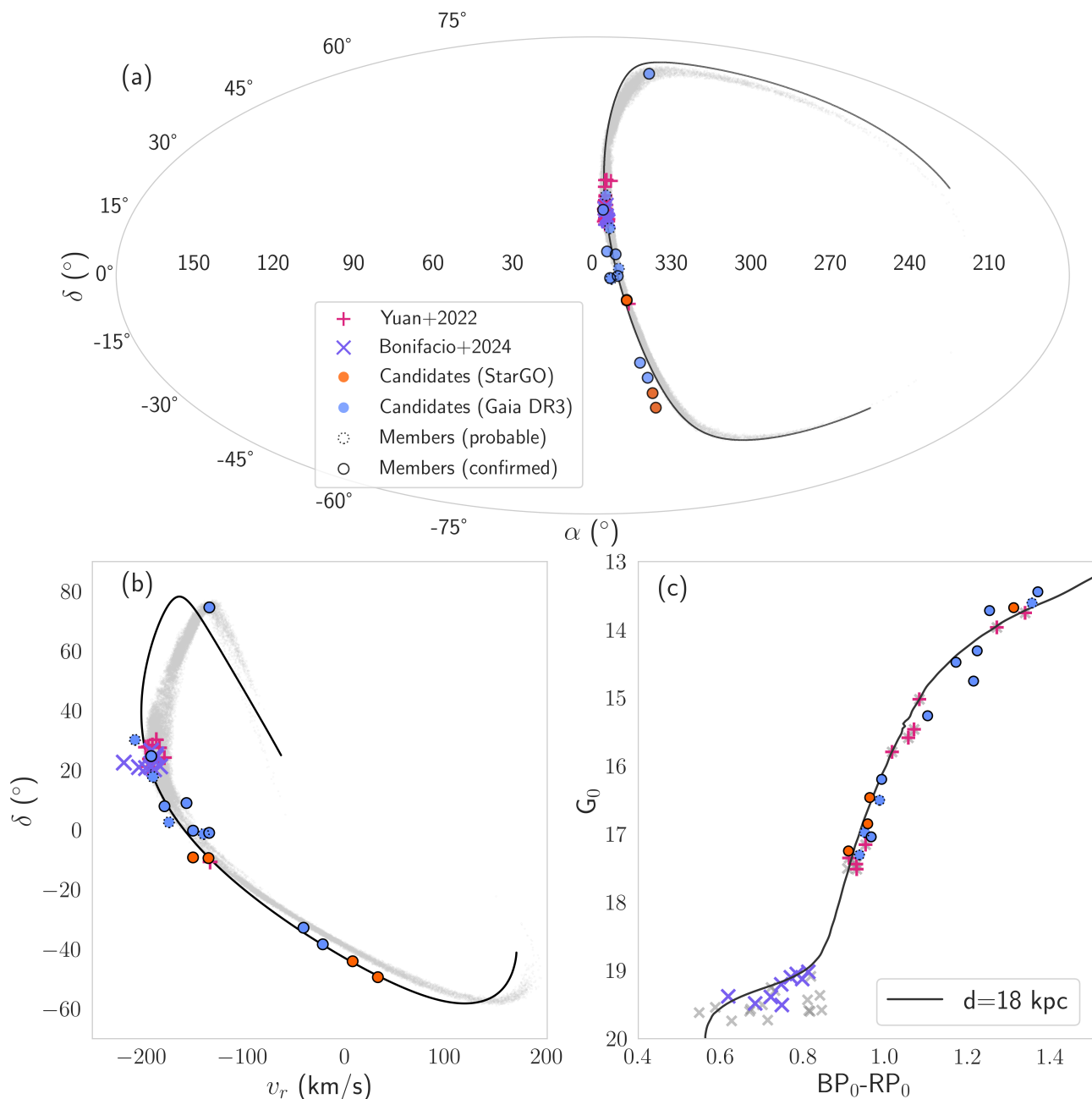


Fig. 2. (a) On-sky projection of the updated sample of C-19 stream members. Previously identified members are represented by magenta (Yuan et al. 2022b) and purple crosses (Bonifacio et al. 2024). The solid black line corresponds to the C-19 orbit derived by Ibata et al. (2023) and the small gray dots represent the simulated stream from Errani et al. (2022). Candidates identified from the fusion of StarGO and STREAMFINDER are plotted as orange circles and the candidates identified using a star-by-star search of photometric metallicity catalogues after *Gaia* DR3 are plotted as blue circles. All shown members have radial velocities consistent with the orbit as shown in panel (b). Stars that have spectroscopic $[Fe/H] < -3.0$ are considered as members and are highlighted with solid black circles. The other stars are probable members and highlighted by dotted circles (see text for more details). (c) Color-magnitude diagram of all the C-19 members, previously identified or from this study and this study. The gray crosses denote candidate members without radial velocity information (Yuan et al. 2022b). The solid black line here represents the 12-Gyr isochrone with $[Fe/H] = -2.2$ from the PARSEC model (Bressan et al. 2012; Fu et al. 2018).

lation (0.17 dex), yielding a typical uncertainty of ~ 0.2 dex in metallicity for this method.

The metallicities reported in this work come from these two methods as well as from spectra with different resolutions. Thus, a consistency check is necessary. We first compare the metallicities of the nine stars with high S/N HR spectra derived using

the two methods described above. These stars are color coded by S/N in the top panel of Fig. 3. By taking into account the uncertainties, the $[Fe/H]$ metallicities based on the Fe lines and $[Fe/H]_{CaT}$, derived from the CaT lines, are close to the one-to-one line. The most discrepant star (2640793013114783872) corresponds to the lowest S/N spectra ($S/N_1 = 7$ in Tab. 1), for

Table 1. Stellar parameters for the new C-19 member stars

Gaia ID	RA ($^{\circ}$)	Dec ($^{\circ}$)	G	Telescope/Instrument	t_{exp} (s)	S/N_1^a	S/N_2^b	v_r (km s^{-1})	$\delta(v_r)$ (km s^{-1})
2758373652717936640	354.57313	9.03539	14.6	SDSS	N/A			-156.88	0.17
2288313499629002624 [†]	298.74545	74.65642	14.1	Subaru/HDS	600	48	23	-134.29	0.67
2606388641446500864	347.06778	-9.21263	17.4	Magellan/MIKE	1200	8	39	-150.44	0.98
2606242131522123520	347.04803	9.42817	17.0	Magellan/MIKE	1200	14	46	-135.14	0.92
6600784780223506944	339.90245	-32.79367	13.5	Magellan/MIKE	600	27	119	-41.15	0.52
6559328209695612544	327.68642	-49.38001	13.7	Magellan/MIKE	600	37	161	+32.42	0.54
6594796290142997376	335.47287	-38.35307	14.5	Magellan/MIKE	600	34	127	-22.09	0.51
6567859904530795904	331.53238	-44.04167	16.5	Magellan/MIKE	1800	16	68	+7.45	0.83
2641204161744171392	353.47032	-0.97001	14.9	VLT/UVES	600	9	72	-134.49	0.70
2852330082409525760	355.83105	24.77643	15.3	VLT/UVES	600	5	34	-191.79	0.54
2760807387346283648	351.31022	7.96339	16.4	VLT/UVES	600	4	36	-178.60	0.64
2871048855556252160	354.48420	30.22392	16.7	VLT/UVES	600	2	19	-207.64	0.61
2658115921889849472	350.14296	2.58381	17.1	VLT/UVES	600	3	14	-172.47	0.83
2644950674600720512	350.57152	-0.22855	17.1	VLT/UVES	600	8	54	-150.23	0.98
2640793013114783872	352.99372	-1.34662	17.4	VLT/UVES	600	7	44	-140.23	0.70

Notes. Star ([†]) has spectra from both Subaru/HDS and INT/IDS, and the radial velocity is derived from the Subaru spectra. ^(a) S/N per 0.05 Å measured at 5863–5865 Å. ^(b) S/N per 1 Å measured at 8639–8644 Å.

Table 2. Metallicities for the new C-19 member stars

Gaia ID	T_{eff} (K)	$\delta(T_{\text{eff}})$ (K)	$\log g$	$\delta(\log g)$	v_t (km s^{-1})	M_{K_s}	$\delta(M_{K_s})$	[Fe/H]	[Fe/H] _{CaT}	Member
2758373652717936640	4762	56	1.33	0.13		-3.90	+0.31		-3.14	Y
2288313499629002624 [†]	4740	52	1.27	0.12	+2.31	-4.03	0.29	-3.37	-3.35	Y
2606388641446500864	5479	110	3.13	0.21	1.31	+0.42	0.51	-3.12	-2.93	Y
2606242131522123520	5260	110	2.59	0.30	1.60	-0.90	0.71	-3.07	-3.07	Y
6600784780223506944	4552	38	0.83	0.09	2.46	-5.04	0.21	-3.29	-3.42	Y
6559328209695612544	4668	51	1.11	0.12	2.40	-4.40	0.28	-3.25	-3.17	Y
6594796290142997376	4812	56	1.45	0.13	2.22	-3.62	0.31	-3.28	-3.29	Y
6567859904530795904	5289	81	2.67	0.22	1.56	-0.70	0.54	-3.30	-3.03	Y
2641204161744171392	4832	76	1.49	0.18	2.20	-3.50	0.43	-3.29	-3.39	Y
2852330082409525760	4957	80	1.74	0.26		-2.93	0.63		-3.35	Y
2760807387346283648	5232	88	2.51	0.24		-1.08	0.58		-3.20	Y
2871048855556252160	5260	93	2.59	0.25		-0.89	0.61		-2.93	P
2658115921889849472	5412	103	2.99	0.25		+0.07	0.60		-2.61	P
2644950674600720512	5224	109	2.49	0.30		-1.12	0.71		-3.27	Y
2640793013114783872	5417	111	2.99	0.26	1.39	+0.08	0.62	-2.59	-3.02	P

Notes. Star ([†]) has spectra from both Subaru/HDS and INT/IDS, which give [Fe/H] and [Fe/H]_{CaT} respectively. Stars denoted by "Y" are confirmed C-19 members that have either [Fe/H] or [Fe/H]_{CaT} within the systematic uncertainty of the C-19 stream (0.2 dex). Those denoted by "P" are probable members that have metallicities beyond the systematic uncertainty.

which both methods may still work. Excluding this low- S/N star, the overall comparison shows that metallicities derived from these two methods are consistent within ~ 0.2 dex. The metallicities derived from the Fe lines for the eight stars also agree well with the mean value of $[\text{Fe}/\text{H}] = -3.38 \pm 0.06(\text{stat.}) \pm 0.20(\text{sys.})$ reported by [Martin et al. \(2022b\)](#), represented by the purple dashed lines and transparent bands in the top panel of Fig. 3.

We then compare the metallicities for the same stars that are derived from spectra of different resolutions as well as from these two methods. There are three stars for which we can do this comparison. In the middle panel of Fig. 3, [Fe/H] represents the measurements from Fe lines using the different HR spectra while [Fe/H]_{CaT} shows estimates using low-

to-medium spectra from INT/IDS with $R \sim 8\,000$, covering the CaT region. The different values for these three stars (yellow and magenta symbols) agree well with each other. Here, the two stars with VLT/UVES spectra are existing C-19 members, Pristine 355.32+27.59 (2865251577418971392) and Pristine 354.96+28.47 (2866151046649496832), from the C-19 discovery study ([Martin et al. 2022b](#)). The other star that has one Subaru/HDS spectrum and one INT/IDS spectrum is a new member confirmed in this study.

To summarize this section, we selected sixteen candidate members of the C-19 stream based on their kinematics in Sec. 2 and confirmed twelve new members that have spectroscopic metallicities consistent within the systematic uncertainty (0.2

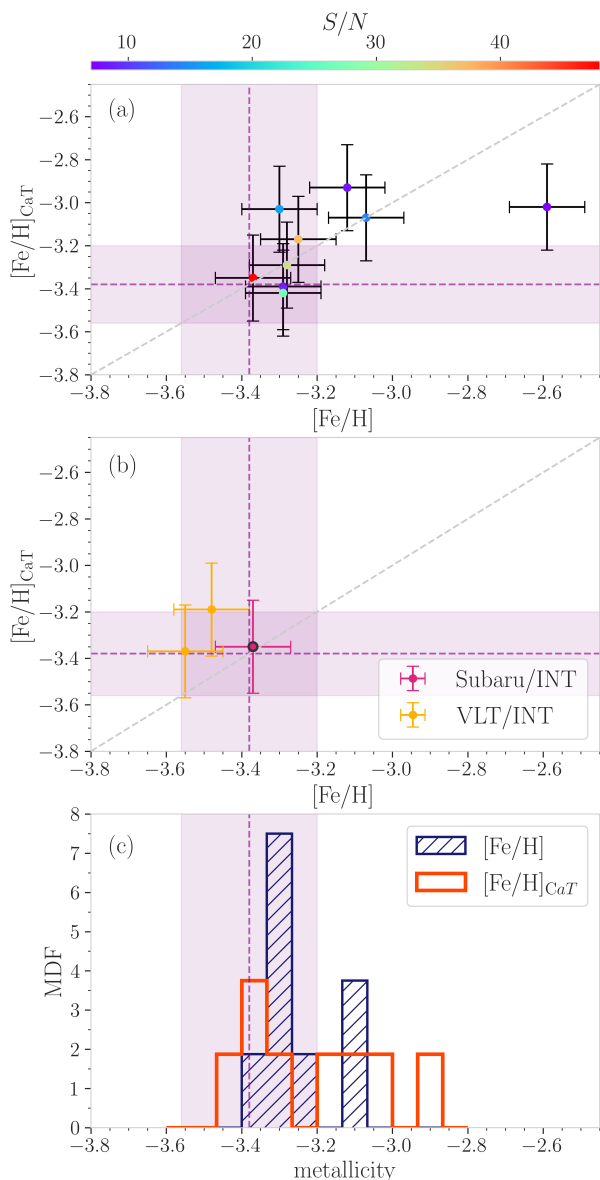


Fig. 3. Metallicities of the C-19 members. (a) Comparison of the metallicities derived from the two methods for the same spectra of the nine stars (blue) that have high S/N HR spectra. The symbols are color-coded by S/N_1 (Tab. 1). The purple dashed line and the bands denote the mean metallicity of the stream ($[\text{Fe}/\text{H}] = -3.38$; Martin et al. 2022b) and its associated systematic uncertainty (0.20 dex). (b) Comparison of the metallicities derived from the HR spectra using Fe lines and the low-to-medium spectra using Ca triplet equivalent widths for three C-19 stars. The two existing member stars in Yuan et al. (2022b) with VLT/UVES spectra are plotted with yellow symbols and the new member with a Subaru/HDS spectrum is shown in magenta. (c) MDFs of $[\text{Fe}/\text{H}]$ and $[\text{Fe}/\text{H}]_{\text{CaT}}$, which are as the blue and orange histograms, respectively.

dex) of the C-19 stream (Martin et al. 2022b) when we take into account the uncertainties of our methods. We plot the metallicity distributions (MDFs) of the newly confirmed members in the bottom panel of Fig. 3, where the blue and orange histograms denote the MDFs of $[\text{Fe}/\text{H}]$ and $[\text{Fe}/\text{H}]_{\text{CaT}}$ respectively. There are three stars with metallicities beyond the systematic uncertainty of the C-19 stream, which are not included in the MDFs. These stars still all have low-metallicity values (< -2.5) and are

marked as ‘probable members’ in Tab. 2, and highlighted by dotted circles in Fig. 2 and Fig. 4. We can see the probable members are not further away from the orbit than the confirmed ones, and they have similar confidence in membership shown in kinematic space. This may suggest that there was an additional, slightly more metal-rich population in the C-19 progenitor. Intriguingly, this result is similar to those of Bonifacio et al. (2024) for turnoff stars in the main body of C-19. However, these stars also all have low S/N spectra and we cannot rule out that the low S/N is unduly affecting our results. These stars require higher S/N spectra to confirm their metallicities.

4. Velocity Dispersion, Width, Mass

Based on the full sample of 22 confirmed members with precise radial velocities, 10 stars from Yuan et al. (2022b) and 12 stars in Sec. 3, we are able to re-evaluate the dynamical properties of C-19. Here, we first rotate the equatorial coordinates to a set of stream coordinate (ϕ_1, ϕ_2) , following the technique presented in Koposov et al. (2010) and adopting the pole and zero-point of the main body of the stream ($\alpha_0 = 354.356^\circ$, $\alpha_{\text{pole}} = 81.45^\circ$, $\delta_{\text{pole}} = -6.346^\circ$) from Ibata et al. (2023). The resulting projection of the sample is displayed in Fig. 4, along with that of the stream orbit, from the same study, that is simultaneously fitted to 29 streams, for an isolated axisymmetric Milky Way potential (Ibata et al. 2023). We then calculate the offsets in velocity ($\Delta v = v_r - v_{r,\text{orbit}}(\phi_1)$) and perpendicular angular distance ($\Delta\phi_2 = \phi_2 - \phi_{2,\text{orbit}}(\phi_1)$) with respect to the orbit. As in Yuan et al. (2022b), we use the formalism of Martin et al. (2018) to infer the mean and dispersion of both quantities, and in this work we obtain $\sigma_v = 11.1^{+1.9}_{-1.5} \text{ km s}^{-1}$ shown in Fig. 5. Among all the members, the star above the disk has the largest offset from the orbit, as shown in the bottom panel of Fig. 4. By excluding this star, the velocity dispersion is only slightly smaller: $\sigma_v = 9.1^{+1.6}_{-1.3} \text{ km s}^{-1}$. To estimate the stream width, we use the densest part of the stream, i.e., the main body located close to the apocentre with the distance around 20 kpc. The dispersion in angular distance is $\sigma_{\phi_2} = 0.61^{+0.17}_{-0.12}$, and the stream width is translated to be ~ 200 pc. These new results clearly show that, over the 100° traced by the updated sample, the C-19 stream is even hotter than previously found. Previous studies focused on the main body of C-19 and gave a velocity dispersion of $6.2^{+2.0}_{-1.4} \text{ km s}^{-1}$, a stream width of ~ 159 pc (Yuan et al. 2022b), and a velocity dispersion of $5.9^{+3.6}_{-5.9} \text{ km s}^{-1}$ for sub-giants (Bonifacio et al. 2024).

The top panel of Fig. 4 shows that members brighter than $G = 16.0$ (orange circles) are nearly evenly distributed along the orbit and become just slightly more clustered in the main body, where seven bright stars are located. There are now thirteen confirmed bright members ($G < 16.0$), which has doubled the previous number of known members presented by Yuan et al. (2022b). There is no reason to expect significant parts of the streams have been missed at this stage as stream segments with similar significance and similar orbital properties as C-19 should have been found using our search method in dynamical space by combining StarGO and STREAMFINDER. This is particularly true beyond the current extent of the stream, in the Galactic caps (Fig. 2), where it is easier to isolate streams because of their higher contrast with the Milky Way stellar populations. The one place where parts of the stream could still be evading detection is behind the Milky Way disk, north of the main body of C-19. The upcoming *Gaia* DR4 with deeper BP/RP spectra as well as further extensions of the Pristine footprint in this direction should help search for the presence of C-19 in this low-latitude region.

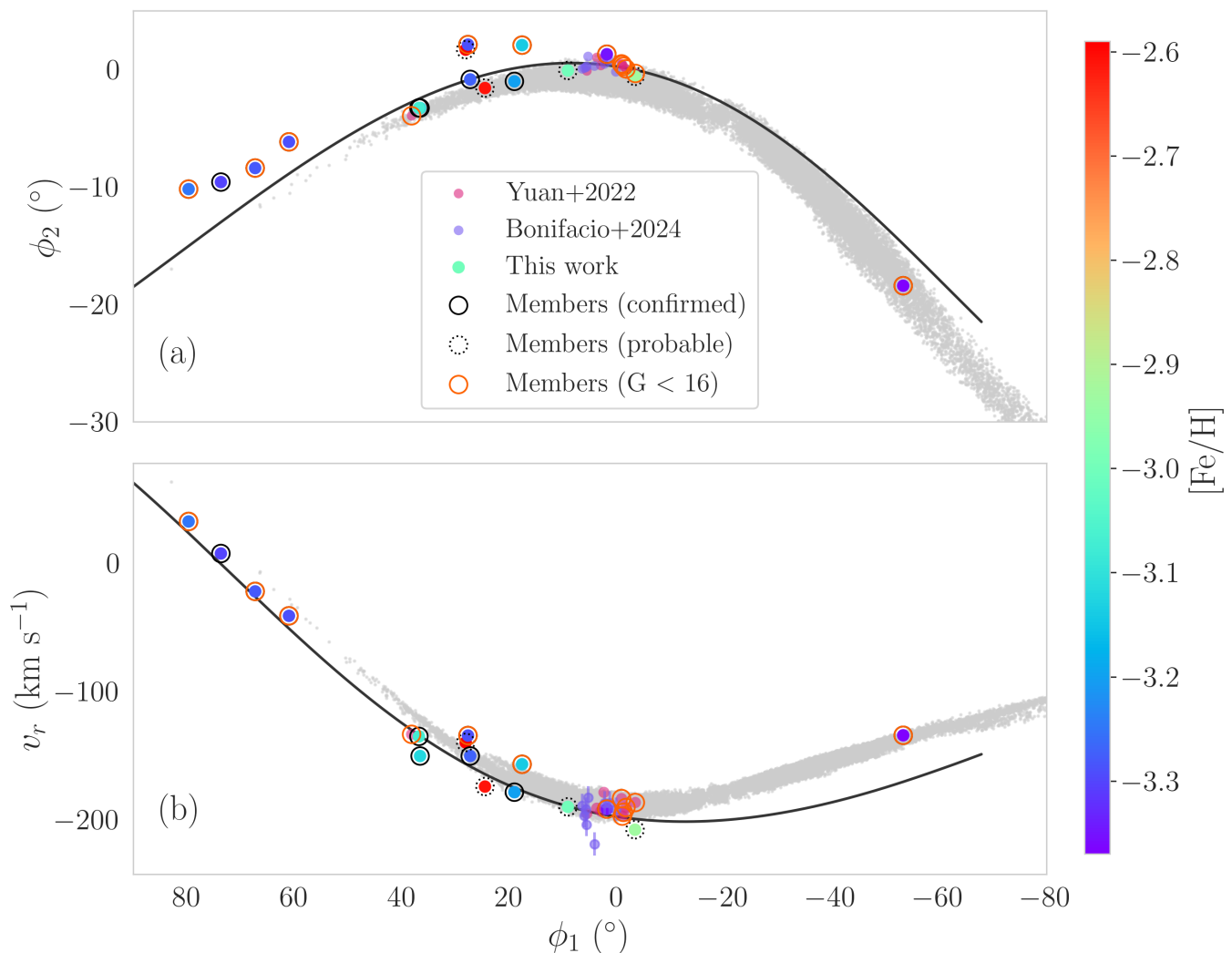


Fig. 4. (a) Spatial distribution of the C-19 stream members with radial velocity measurements in the (ϕ_1, ϕ_2) coordinate. Similar to Fig. 2, the members from previous studies are plotted as transparent red and purple circles (Martin et al. 2022a; Yuan et al. 2022b; Bonifacio et al. 2024), as well as the derived orbit (Ibata et al. 2023), and the simulated stream (Errani et al. 2022). All the candidates from this work are color coded by their spectroscopic metallicities. The confirmed members have metallicities below -3 , which are highlighted with solid black circles. The rest are probable members denoted by dotted circles. Among all the confirmed members, those brighter than $G = 16$ are further highlighted with orange circles, which are just slightly clustered in the main body (b) The C-19 stream in the (ϕ_1, v_r) space, where the radial velocity measurements are taken from Yuan et al. (2022b); Bonifacio et al. (2024) and this work.

With the current extension of the stream and the star-by-star search in *Gaia*, described in Sec. 2.2, we have checked all the low-metallicity stars in the *Pristine-Gaia* synthetic catalogue along the stream orbit with compatible proper motions down to $G \approx 16.0$ (Martin et al. 2024). Assuming the resulting sample of members is close to complete, we can update the estimated mass of the C-19 stream. This mass will still be a lower limit but should be closer to the true mass of the C-19 progenitor than earlier estimates ($> 3.5 \times 10^3 L_\odot$ or $0.8 \times 10^4 M_\odot$) based on the main body of the stream (Martin et al. 2022a). By summing the fluxes of all the stars brighter than $G = 16.0$ along the giant branch, the total luminosity is $1.8 \times 10^4 L_\odot$ after correction for the unobserved fainter stars using the luminosity function associated with the PARSEC isochrone mentioned above (Bressan et al. 2012; Fu et al. 2018) and using a Kroupa initial mass function (IMF Kroupa 2001, 2002). Assuming a mass-to-light ratio $M/L = 2-3$, typical of very old stellar populations (Maraston 2005), the mass

of C-19 is $\sim 3.7 - 5.5 \times 10^4 M_\odot$, which, unsurprisingly given the much larger number of confirmed bright C-19 members, is significantly larger than the previous estimate. Note that a different IMF would also affect the derived mass-to-light ratio (e.g., Cappellari et al. 2012). There is observational evidence suggesting that top-heavy IMFs are favored in extremely dense star-forming regions, such as the 30 Doradus star-forming region in the Large Magellanic Cloud (Schneider et al. 2018) or star burst galaxies at redshift $\sim 2-3$ (Zhang et al. 2018; Guo et al. 2024). The C-19 progenitor was very likely a globular cluster, which could have been born in a similar environment of dense clouds and intense star-formation. Assuming a top-heavy IMF calibrated for very metal-poor GCs (Marks et al. 2012), the mass-to-light ratio further increases by a factor ~ 1.3 , which would result in an even larger progenitor mass of $5 - 8 \times 10^4 M_\odot$.

As was discussed in Yuan et al. (2022b), the typical velocity dispersion of a GC stream is less than 5 km s^{-1} (Li et al. 2022b).

However, with more spectroscopic data available for streams, more have been found to be dynamically hot. For example, the recent velocity dispersion of GD-1 is $\sim 7 - 29 \text{ km s}^{-1}$ (Malhan et al. 2019; Ibata et al. 2023), despite a progenitor mass of $\sim 10^5 M_{\odot}$ (Ibata et al. 2020). It has been suggested that this progenitor was accreted and pre-processed inside a dark matter subhalo (Carlberg 2020; Malhan et al. 2021; Carlberg & Agler 2023). In the case of C-19, the experiment of pre-processing a globular cluster in a dark matter subhalo remains a good explanation for the observed velocity dispersion (Errani et al. 2022). A recent study by Carlberg et al. (2024) shows the tidal heating of a cold globular cluster stream by Λ CDM dark subhalos are able to increase the large velocity dispersion to values similar to the dispersion measured in the main body of C-19 ($\sim 6 \text{ km s}^{-1}$). But, the heated velocity dispersion values stay short of the velocity dispersion we find from the larger sample presented in this paper ($\sim 11 \text{ km s}^{-1}$). Other possible scenario to explain the high velocity dispersion would include heating by giant molecular clouds (see e.g., Amorisco et al. 2016) or, as recently showed from detailed N-body simulations of globular clusters (Wang 2020; Gieles et al. 2021; Wang et al. 2024), the presence of black holes could enhance the relaxation and disruption of a GC, leading to a larger initial line-of-sight velocity dispersion. Born in a dense and extremely metal-poor region, the C-19 progenitor may also favor a top-heavy IMF, and the strong stellar feedback from over-abundant massive stars could cause the cluster to be born dynamically hot in the first place (Wang 2020; Wang et al. 2021). Finally, unresolved binaries could also lead to an artificially large velocity dispersion. From the eight C-19 stars with radial velocity measurements from Gaia, there is no noticeable variation in velocities from our measurements and those from Gaia RVS (Katz et al. 2023). We do not see unexpectedly large uncertainties in each measurement either. Note that each star only has one precise velocity measurement from our follow-up and the mean value from Gaia DR3. Therefore, future multi-epoch spectroscopic observations will be crucial to quantify the contribution of binaries to the observed properties of C-19.

5. Conclusions

In this work, we searched for potential members of C-19 in dynamical space by applying StarGO to the low-significance stream stars from STREAMFINDER. With this technique, we found 4 new C-19 members, located 30° and 60° south from the main body. After Gaia DR3, we perform a star-by-star searches along the C-19 orbit using very low-metallicity star catalogues from the Pristine survey (both based on genuine Pristine data and on Gaia XP spectra; Martin et al. 2024). In total, we confirm twelve new members of the C-19 stream through high-resolution spectroscopy. All new members have velocities compatible with predictions from the orbit based on the main body of the stream (Martin et al. 2022a; Ibata et al. 2023), and their metallicities are, within the uncertainty of measurements, in agreement with the extremely metal-poor mean metallicity of the stream.

Our search for C-19 members in the bright regime ($G < 16.0$) utilizes the all-sky Gaia data and we therefore expect that the distribution of these bright stars gives a relatively fair representation of the extent of the stream. Its main body, where it was originally detected, is centered around $\delta \sim +26^\circ$ (Ibata et al. 2021; Martin et al. 2022b), and remains the densest part but we now show that it continuously extends down to $\delta \sim -15^\circ$ in the South. A separate segment of the stream of four members is located at $\delta \sim -40^\circ$. One single member is found on the other side

of the Milky Way disk, at $\delta = +75^\circ$, in the North. Overall, the C-19 stream is now shown to extend over $\sim 100^\circ$ on the sky. By summing up the fluxes from bright stars along the giant branch ($G < 16.0$), we revise the lower mass limit of the stream significantly upwards to $3.7 - 5.5 \times 10^4 M_{\odot}$. Based on the velocity measurements of all members, accurate at the $\sim 1 \text{ km s}^{-1}$ level, we revise upwards both the velocity dispersion of the stream to $11.1^{+1.9}_{-1.5} \text{ km s}^{-1}$, and its Gaussian width to $\sim 200 \text{ pc}$. The stream is both hotter and more diffuse than previously reported (Martin et al. 2022a; Yuan et al. 2022b).

From a dynamical point of view, it remains a puzzle how to explain the large velocity dispersion with the relative small mass of the stream progenitor. Our suggested scenario of a pre-heating/disruption of C-19 cluster in its own dark-matter halo remains a possibility (Errani et al. 2022). In addition, tidal heating from the interaction of the stream with dark-matter subhalos (Carlberg et al. 2024) or giant molecular clouds are also possibilities. The scenario of a top-heavy IMF would result in an over-abundance of massive stars, whose stellar feedback could lead to a dynamically hotter initial globular cluster immediately after its birth. Finally, the contribution of binary systems to the observed velocity dispersion remains unknown and could significantly inflate it (Wang et al. 2024). It is crucial and timely to obtain multiple spectroscopic observations of known C-19 members to hunt for spectroscopic binaries if we are to understand the dynamical nature of this exceptional stream.

Acknowledgements. ZY, NFM, and RAI acknowledge funding from the European Research Council (ERC) under the European Unions Horizon 2020 research and innovation programme (grant agreement No. 834148). KM was supported by a research grant (VIL53081) from VILLUM FONDEN. This work has made use of data from the European Space Agency (ESA) mission *Gaia* (<https://www.cosmos.esa.int/gaia>), processed by the *Gaia* Data Processing and Analysis Consortium (DPAC, <https://www.cosmos.esa.int/web/gaia/dpac/consortium>). Funding for the DPAC has been provided by national institutions, in particular the institutions participating in the *Gaia* Multilateral Agreement. This research is based in part on data collected at the Subaru Telescope, which is operated by the National Astronomical Observatory of Japan. We are honored and grateful for the opportunity of observing the Universe from Maunakea, which has the cultural, historical, and natural significance in Hawaii. This paper includes data gathered with the 6.5 meter Magellan Telescopes located at Las Campanas Observatory, Chile. This work is based in part on observations collected at the European Organisation for Astronomical Research in the Southern Hemisphere under ESO programme 111.2517.001. The INT/IDS is operated on the island of La Palma by the Isaac Newton Group of Telescopes in the Spanish Observatorio del Roque de los Muchachos of the Instituto de Astrofísica de Canarias. Based on observations obtained with MegaPrime/MegaCam, a joint project of CFHT and CEA/DAPNIA, at the Canada-France-Hawaii Telescope (CFHT) which is operated by the National Research Council (NRC) of Canada, the Institut National des Sciences de l'Univers of the Centre National de la Recherche Scientifique of France, and the University of Hawaii. Funding for SDSS-III has been provided by the Alfred P. Sloan Foundation, the Participating Institutions, the National Science Foundation, and the U.S. Department of Energy Office of Science.

References

- Amorisco, N. C., Gómez, F. A., Vegetti, S., & White, S. D. M. 2016, MNRAS, 463, L17
- Andrae, R., Fouesneau, M., Sordo, R., Bailer-Jones, C. A. L., & Dharmawardena, 2023, A&A, 674, A27
- Aoki, W., Beers, T. C., Lee, Y. S., et al. 2013, AJ, 145, 13
- Argast, D., Samland, M., Gerhard, O. E., & Thielemann, F. K. 2000, A&A, 356, 873
- Bastian, N. & Lardo, C. 2018, ARA&A, 56, 83
- Bernstein, R., Shtetman, S. A., Gunnels, S. M., Mochnecki, S., & Athey, A. E. 2003, in Society of Photo-Optical Instrumentation Engineers (SPIE) Conference Series, Vol. 4841, Instrument Design and Performance for Optical/Infrared Ground-based Telescopes, ed. M. Iye & A. F. M. Moorwood, 1694–1704
- Blanco-Cuaresma, S. 2019, MNRAS, 486, 2075

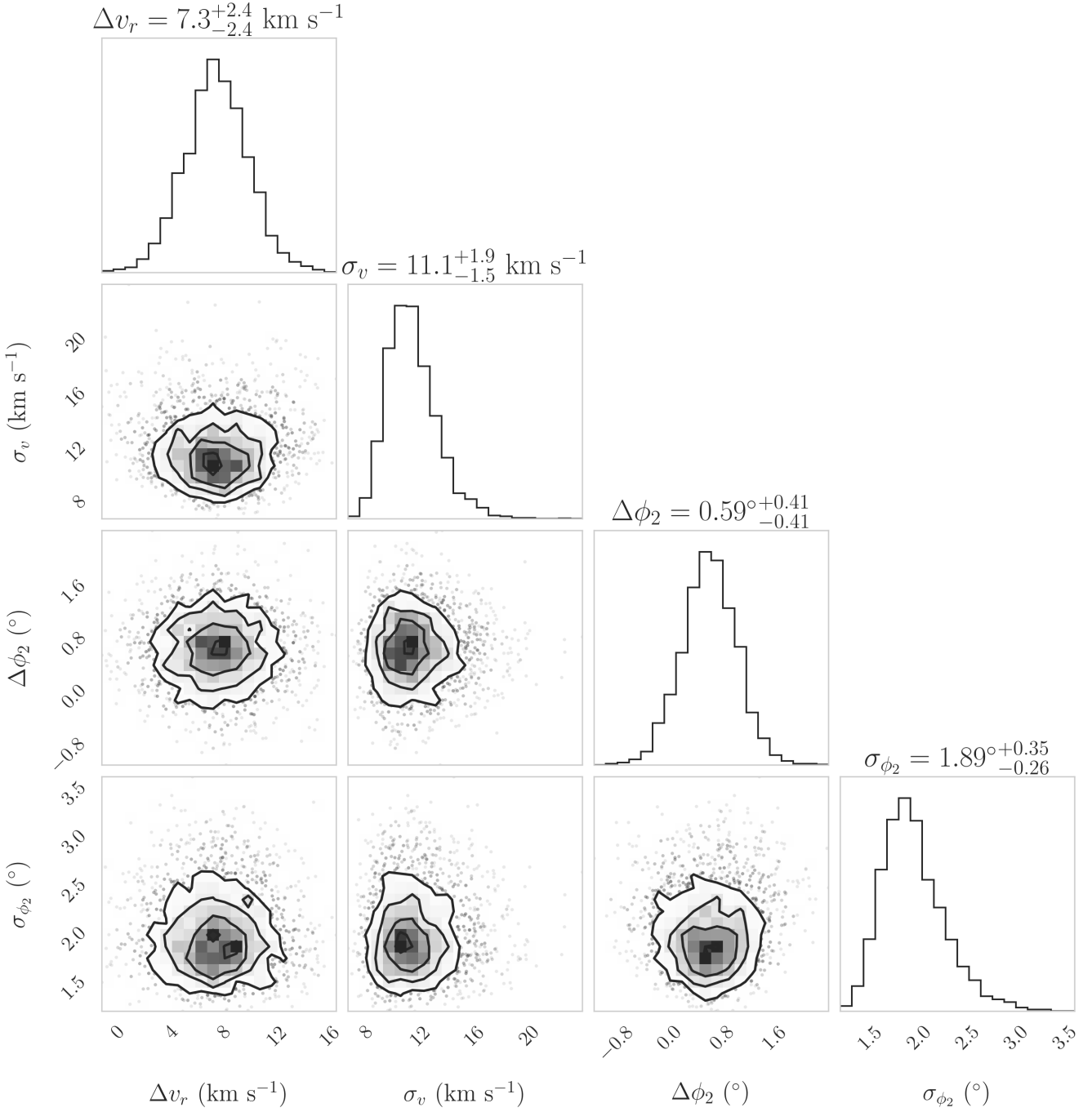


Fig. 5. Probability distribution functions (PDFs) of the mean offsets of the twenty two confirmed C-19 member stars from the orbit in velocity (Δv) and position ($\Delta\phi_2$), along with the corresponding dispersions, σ_v , and σ_{ϕ_2} . The bottom left-hand panels shows the two-dimensional PDF, taken directly from the Markov chain Monte Carlo sampling and the histograms display the marginalized one-dimensional PDFs for the three parameters.

Blanco-Cuaresma, S., Soubiran, C., Heiter, U., & Jofré, P. 2014, *A&A*, 569, A111
Bonifacio, P., Caffau, E., François, P., et al. 2024, arXiv e-prints, arXiv:2412.20776
Bressan, A., Marigo, P., Girardi, L., et al. 2012, *MNRAS*, 427, 127
Cappellari, M., McDermid, R. M., Alatalo, K., et al. 2012, *Nature*, 484, 485
Carlberg, R. G. 2020, *ApJ*, 889, 107
Carlberg, R. G. & Agler, H. 2023, *ApJ*, 953, 99
Carlberg, R. G., Ibata, R., Martin, N. F., et al. 2024, arXiv e-prints, arXiv:2410.22966
Carrasco, J. M., Weiler, M., Jordi, C., et al. 2021, *A&A*, 652, A86
Carrera, R., Pancino, E., Gallart, C., & del Pino, A. 2013, *MNRAS*, 434, 1681
Chabrier, G. 2003, *PASP*, 115, 763

Cutri, R. M., Skrutskie, M. F., van Dyk, S., & Beichman. 2003, *2MASS All Sky Catalog of point sources*.
Dekker, H., D’Odorico, S., Kaufer, A., Delabre, B., & Kotzlowski, H. 2000, in *Society of Photo-Optical Instrumentation Engineers (SPIE) Conference Series*, Vol. 4008, *Optical and IR Telescope Instrumentation and Detectors*, ed. M. Iye & A. F. Moorwood, 534–545
Errani, R., Navarro, J. F., Ibata, R., et al. 2022, *MNRAS*, 514, 3532
Fu, X., Bressan, A., Marigo, P., et al. 2018, *MNRAS*, 476, 496
Gieles, M., Erkal, D., Antonini, F., Balbinot, E., & Peñarrubia, J. 2021, *Nature Astronomy*, 5, 957
Gratton, R., Sneden, C., & Carretta, E. 2004, *ARA&A*, 42, 385
Guo, Z., Zhang, Z.-Y., Yan, Z., et al. 2024, *ApJ*, 970, 136
Gustafsson, B., Edvardsson, B., Eriksson, K., et al. 2008, *A&A*, 486, 951

- Hidalgo, S. L., Pietrinferni, A., Cassisi, S., et al. 2018, *ApJ*, 856, 125
- Huang, Y., Beers, T. C., Wolf, C., et al. 2022, *ApJ*, 925, 164
- Ibata, R., Malhan, K., Martin, N., et al. 2021, *ApJ*, 914, 123
- Ibata, R., Malhan, K., Tenachi, W., et al. 2023, arXiv e-prints, arXiv:2311.17202
- Ibata, R., Thomas, G., Famaey, B., et al. 2020, *ApJ*, 891, 161
- Katz, D., Sartoretti, P., Guerrier, A., et al. 2023, *A&A*, 674, A5
- Kelson, D. D. 2003, *PASP*, 115, 688
- Koposov, S. E., Rix, H.-W., & Hogg, D. W. 2010, *ApJ*, 712, 260
- Kroupa, P. 2001, *MNRAS*, 322, 231
- Kroupa, P. 2002, *Science*, 295, 82
- Li, H., Aoki, W., Matsuno, T., et al. 2022a, *ApJ*, 931, 147
- Li, T. S., Ji, A. P., Pace, A. B., et al. 2022b, *ApJ*, 928, 30
- Malhan, K., Ibata, R. A., Carlberg, R. G., Valluri, M., & Freese, K. 2019, *ApJ*, 881, 106
- Malhan, K., Valluri, M., & Freese, K. 2021, *MNRAS*, 501, 179
- Maraston, C. 2005, *MNRAS*, 362, 799
- Marks, M., Kroupa, P., Dabringhausen, J., & Pawlowski, M. S. 2012, *MNRAS*, 422, 2246
- Martin, N. F., Collins, M. L. M., Longeard, N., & Tollerud, E. 2018, *ApJ*, 859, L5
- Martin, N. F., Ibata, R. A., Starkenburg, E., et al. 2022a, *MNRAS*, 516, 5331
- Martin, N. F., Starkenburg, E., Yuan, Z., et al. 2024, *A&A*, 692, A115
- Martin, N. F., Venn, K. A., Aguado, D. S., & Starkenburg, E. 2022b, *Nature*, 601, 45
- Montegriffo, P., De Angeli, F., Andrae, R., et al. 2023, *A&A*, 674, A3
- Noguchi, K., Aoki, W., Kawanomoto, S., et al. 2002, *PASJ*, 54, 855
- Pietrinferni, A., Hidalgo, S., Cassisi, S., et al. 2021, *ApJ*, 908, 102
- Schneider, F. R. N., Sana, H., Evans, C. J., et al. 2018, *Science*, 359, 69
- Skrutskie, M. F., Cutri, R. M., Stiening, R., & Weinberg, M. D. 2006, *AJ*, 131, 1163
- Snedden, C. 1973, *ApJ*, 184, 839
- Starkenburg, E., Martin, N., & Youakim, K. 2017, *MNRAS*, 471, 2587
- Viswanathan, A., Yuan, Z., Ardem-Arentsen, A., et al. 2024, arXiv e-prints, arXiv:2405.13124
- Wan, Z., Lewis, G. F., Li, T. S., et al. 2020, *Nature*, 583, 768
- Wang, L. 2020, *MNRAS*, 491, 2413
- Wang, L., Fujii, M. S., & Tanikawa, A. 2021, *MNRAS*, 504, 5778
- Wang, L., Gieles, M., Baumgardt, H., et al. 2024, *MNRAS*, 527, 7495
- Yuan, Z., Chang, J., Banerjee, P., et al. 2018, *ApJ*, 863, 26
- Yuan, Z., Malhan, K., Sestito, F., et al. 2022a, *ApJ*, 930, 103
- Yuan, Z., Martin, N. F., & Ibata, R. A. 2022b, *MNRAS*, 514, 1664
- Zavala, J. A., Castellano, M., Akins, H. B., et al. 2024, *Nature Astronomy* [arXiv:2403.10491]
- Zhang, Z.-Y., Romano, D., Ivison, R. J., Papadopoulos, P. P., & Matteucci, F. 2018, *Nature*, 558, 260